Chemical Physics 175 (1993) 171–191
North-Holland

Picosecond dynamics of *n*-hexane solvated trans-stilbene

Christoph Lienau [1], Ahmed A. Heikal and Ahmed H. Zewail
Arthur Amos Noyes Laboratory of Chemical Physics [2], California Institute of Technology, Pasadena, CA 91125, USA

Received 30 April 1993

In this article, we report studies of the time- and frequency-resolved picosecond dynamics of trans-stilbene solvated with one *n*-hexane molecule in a van der Waals complex. Excitations are made to several overtones of a low-frequency intermolecular vibration and to combination bands of these overtones with the symmetric in-plane ethylene bend mode ν_{25} in the S_1 state of two distinct conformers, A and C, of these complexes. A Franck–Condon analysis of these spectra allows a characterization of the potential for this intermolecular mode in the ground and excited electronic state of both conformers. From the time-resolved dynamics of the A-isomer, the three different types of IVR behavior in the cluster, as in the bare molecule, are identified and studied. Single exponential fluorescence decays are observed at low excess energies, showing *no* IVR on the time scale of the lifetime of the molecule. At intermediate energies, between 220 and 260 cm^{-1}, quantum-beat modulated decay profiles indicate *restricted* IVR dynamics. At higher excess energies IVR becomes *dissipative* and biexponential decays are observed. The decrease in the lowest excess energy at which dissipative IVR behavior sets in, from 1200 cm^{-1} in the bare *t*-stilbene molecule to less than 300 cm^{-1} in the complex, is attributed to a large increase in the density of vibrational states of the complex due to the six low-frequency intermolecular vibrations of the cluster. A similar study of the C-isomer reveals that the IVR dynamics become even more accelerated. Excitation of the stilbene mode ν_{25} at 200 cm^{-1} leads to dissipative energy flow from the stilbene molecule into the cluster vibrations within tens of picoseconds, becoming faster for higher excess energies. The results present a nice example of the significant impact that low-frequency "solvent-like" cluster vibrations have on the dynamics of vibrational energy redistribution and the coherent transfer of vibrational energy between the solute and the cluster modes.

1. Introduction

The dynamics of intramolecular vibrational-energy redistribution (IVR) can generally be divided according to three different regimes [1–5]: *no* IVR at very low vibrational energies; *restricted* IVR in an intermediate energy range, characterized by quantum-beat modulated fluorescence decay profiles; and *dissipative* IVR, occurring within tens of picoseconds, at higher energies. These regions of IVR have been identified and studied in the prototype systems anthracene [1,2] and trans-stilbene [3–5] by resolving the picosecond dynamics (in time and frequency) of beam-cooled molecules. A number of other aromatic molecules have been shown to exhibit the same kind of behavior, and these include perylene [6], fluorene [7], azulene [8], *n*-alkyl anilines [9], 1-methylindole [10], naphthol [11], *p*-cyclohexylaniline [12,13], 2,5-diphenylfuran [14], deuterated analogs of anthracene [15], and derivatives of *t*-stilbene [16]. There is yet no quantitative theory to predict the onset of IVR in these large systems, but one can relate the role of the two key factors, the density-of-states and the coupling matrix elements, to the dynamics.

It is interesting to examine IVR in van der Waals complexes as, due to the large number of low-frequency intermolecular modes, the density-of-states is very high, and, unlike small systems [17–20], both intramolecular and intermolecular energy flow are possible.

One class of these systems involves complexes of aromatic molecules with one or more rare gas atoms. Such complexes are characterized by a low binding energy, on the order of some hundred cm^{-1}, so that IVR is generally followed by fast vibrational predissociation of the complex [21–23]. The time scale of IVR depends on the coupling of the initially excited mode to other modes in the molecule. In Rettschnick's

[1] Deutsche Forschungsgemeinschaft Postdoctoral Fellow.
[2] Contribution No. 8790.

original work on tetrazine/argon complexes [24], IVR was found to occur on a time scale of several nanoseconds at excess vibrational energies of 500 to 800 cm^{-1}. This is in marked contrast to the extremely slow energy redistribution in the electronic ground state of these clusters [25]. Experiments on anthracene [22] and stilbene [21] rare gas complexes show that in the energy range from 300 to 800 cm^{-1} IVR is extensive within hundreds of picoseconds, considerably faster than in the bare molecule. This was attributed to an increase in the density of ro-vibrational states caused by the low-frequency intermolecular vibrations. Topp's group [14] observed a quantum-beat modulated fluorescence decay in 2,5-diphenylfuran/argon complexes, indicating that restricted IVR occurs on a time scale of some hundreds of picoseconds.

For some "solute/solvent" clusters, the binding energy is much larger than that of the rare gas systems. IVR should be observable without dissociating the complex, and these systems should provide an opportunity to test the influence of intermolecular modes and solute–solvent interactions on IVR. One interesting example came from a study [26,27] by the group of Topp. They found that the vibrational-energy redistribution from molecular into cluster modes is more than one order of magnitude slower in the case of perylene/naphthalene than for perylene/benzene or perylene/alkane complexes. These results are not expected if intermolecular modes are the dominating states of the redistribution in both complexes.

Stilbene solvated by hexane has many attractive features, and here we examine the picosecond dynamics of IVR in the 1:1 complex using time- and frequency-resolved picosecond fluorescence spectroscopy. The rich fluorescence excitation spectrum [28] of these complexes allows us to investigate the dynamics of molecular stilbene modes in addition to several overtones of a low-frequency intermolecular vibration and combination bands of molecular and cluster vibrations. Consequently, the energy flow from the stilbene molecule into the cluster as well as between different intermolecular modes can be examined. In the studies reported here, all three regions of IVR were observed and the dynamics reflect the influence of "solvent-like" modes on the flow of vibrational energy. The fact that bare stilbene dynamics are known [3–5] makes the comparison in this study particularly important.

2. Experimental

The molecular beam, the laser system and the time-correlated single photon counting data acquisition have been described in previous publications [1,29]. Briefly, mixed clusters were produced in a seeded supersonic jet expansion. Trans-stilbene (Aldrich, 96% purity, used without further purification) was placed in the sample compartment of a Pyrex nozzle ($D \approx 70$ μm) and heated to ≈ 100°C. The helium expansion gas was maintained at ≈ 70 psi and contained about 1% of *n*-hexane vapor. A heatable stainless steel reservoir filled with *n*-hexane (Aldrich, UV spectroscopy grade, 99% purity) was connected to the gas supply via a tee and a short capillary ($\varnothing = 3$ mm, $L = 50$ mm), so that the hexane vapor above the liquid had to diffuse into the rare gas stream through the capillary. In this way, the partial pressure of *n*-hexane (≈ 50 mbar) in the expansion gas was considerably lower than the hexane vapor pressure above the liquid. Heating the hexane sample provided control over the beam composition and allowed suppression of larger clusters ($n \geq 2$).

The supersonic beam was crossed at ≈ 2 mm downstream from the nozzle with the frequency-doubled output of a synchronously pumped, cavity-dumped dye-laser (Spectra Physics), operating at a repetition rate of 4 MHz. The UV pulses, which were generated in a $LiIO_3$ crystal, had a temporal width of 15 ps fwhm and a spectral bandwidth of 5 cm^{-1}. The laser-induced fluorescence was collected at right angles to both the laser and the molecular beam through a collimating lens, and was focused by a second lens onto the entrance slit of a microprocessor controlled 0.5 m monochromator (SPEX Industries 1870). At the exit slit, single photons were detected by a microchannel plate photomultiplier tube (Hamamatsu R-2287 U), whose output was amplified (Hewlett Packard HP 8447), fed through a constant-fraction discriminator (Tennelec CFD 545) and used to trigger the start channel of a biased time-to-amplitude converter (EG&G TAC 457). The stop channel of the TAC was triggered by the delayed and amplified output of a fast photodiode detecting the visible laser

pulses. The TAC output was fed to a multichannel analyzer in pulse-height-analysis mode, producing a histogram of photon arrival times. This data was transferred to a PDP11/23 computer for storage and analysis.

The instrument response was measured by advancing the tip of the nozzle close to the laser beam and detecting the scattered light. The average full-width at half-maximum (fwhm) of the detected response function was 75 ps. The time calibration of the TAC was provided by the very stable rf-source of the mode locked Ar^+ laser. This calibration was checked by reproducing the precisely known recurrence period of the polarization analyzed fluorescence of the $S_1(v=0) \leftarrow S_0(v=0)$ transition in trans-stilbene [30]. The time-resolved fluorescence decays were fitted using a nonlinear least-squares curve fitting routine [31,32] based on Marquardt's algorithm [33]. The instrument response function used for convolution was monitored after each fluorescence decay curve.

3. Spectra and the potential

3.1. Fluorescence excitation spectrum

The fluorescence excitation spectrum of the first excited electronic state (S_1) of *t*-stilbene/*n*-hexane (1:1) complexes, which has recently been reported by Lienau et al. [28], is reproduced in fig. 1. It reveals the presence of three structural isomers, labeled A, B, and C, whose origins are red-shifted by 380 cm^{-1} (A-isomer), 348 cm^{-1} (B-isomer) and 265 cm^{-1} (C-isomer) relative to the electronic origin of trans-stilbene [3,34] at 32234.744 ± 0.002 cm^{-1} [35]. The assignment of the isomers is taken from ref. [28], where it is based on a series of measurements of the fluorescence excitation spectrum as a function of hexane concentration and on an analysis of vibrational spacings in the spectra. The intensity of the origin transition of the B- and C-isomer relative to the intensity of the A-isomer is 0.04 and 0.5, respectively. The prominent feature of the excitation spectrum is a long progression of one optically active low-frequency cluster mode (labeled X) with a spacing of $\bar{\nu}=20\pm0.5$ cm^{-1} for the A-isomer (B: $\bar{\nu}=18\pm1$ cm^{-1}, C: $\bar{\nu}=17\pm0.5$ cm^{-1}) [28]. Following the interpretation given by Mangle et al. [36] for

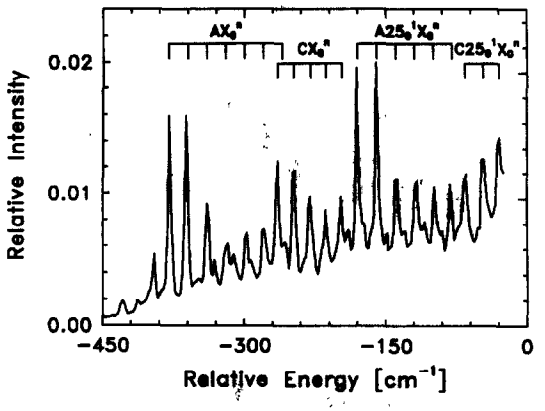

Fig. 1. Fluorescence excitation spectrum of trans-stilbene/*n*-hexane complexes as reported by Lienau et al. [28]. The energy is given in cm^{-1} relative to the 0_0^0-transition of *t*-stilbene, which has a relative intensity of 1.0. The progressions AX_0^n and $A25_0^1X_0^n$ for the A-isomer and CX_0^n and $C25_0^1X_0^n$ for the C-isomer are highlighted in the spectrum.

the low-frequency mode observed in the excitation spectrum of 2,5-diphenylfuran/hexane (1:1) complexes, this mode is presumably related to a torsion motion of the alkane molecule around an axis perpendicular to the plane of the stilbene molecule. For each isomer this progression is found again shifted by 200 cm^{-1} to the blue due to the excitation of a combination of the symmetric in-plane, in-phase vibration ν_{25} [37,3,34] of the stilbene molecule and the low-frequency cluster mode X.

Potential energy calculations based on atom–atom pair potentials [36], together with measurements of the rotational constants of 2,5-diphenylfuran/alkane complexes using rotational coherence spectroscopy [38,27] provide evidence that, in this case, the long axis of the diphenylfuran and alkane molecules are oriented parallel to each other. We assume that a similar structure will be the most energetically favorable for stilbene/hexane. Preliminary experiments on the rotational coherence spectroscopy of these complexes [28] are in agreement with the structure shown in fig. 2, where the hexane molecule is located in a plane parallel to that spanned by the two phenyl rings, with its long axis parallel to the long axis of trans-stilbene. Semiempirical calculations to confirm this structure are given in the Appendix. These calculations provide an *estimate* of the dissociation energy of these clusters.

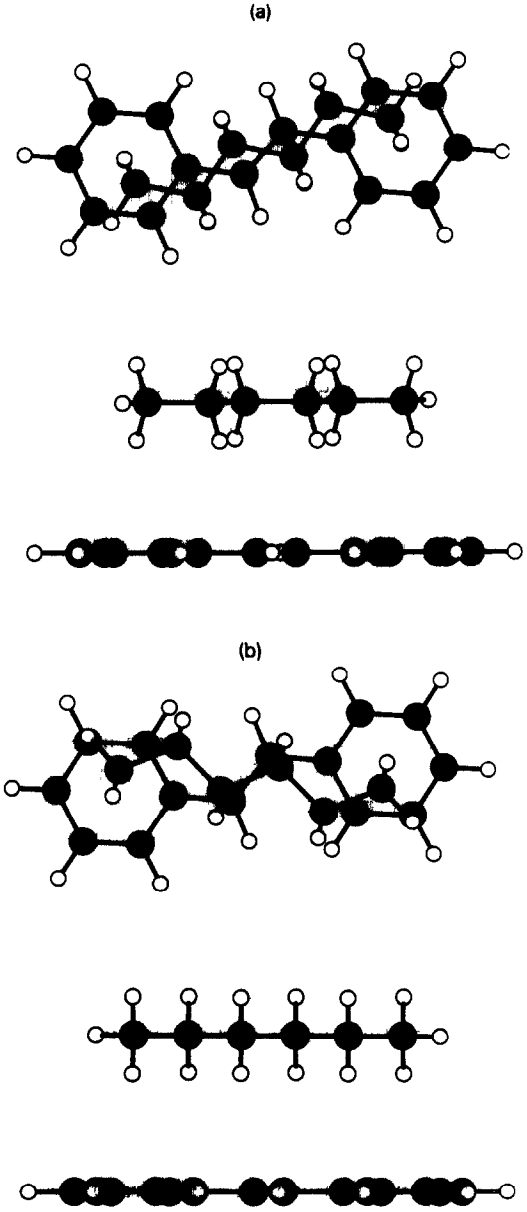

Fig. 2. Structure of the A-isomer (a) and C-isomer (b) of *t*-stilbene/*n*-hexane (1:1) complexes (see text and Appendix).

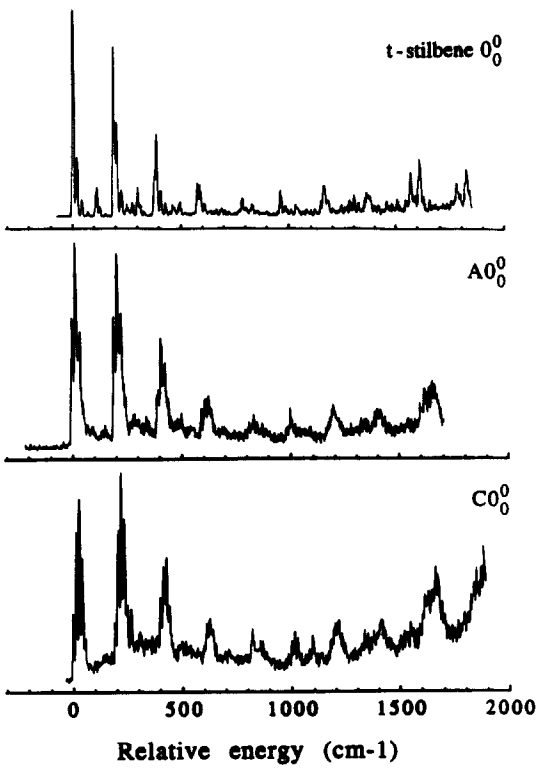

Fig. 3. Dispersed fluorescence spectra of trans-stilbene and the two isomers A and C excited to the origin 0_0^0 in their S_1-electronic state. The energy is given in cm^{-1} relative to the electronic origin of trans-stilbene (32235 cm^{-1}), A-isomer (31855 cm^{-1}) and C-isomer (31970 cm^{-1}), respectively. All three spectra have been recorded under the same experimental conditions: *t*-stilbene temperature $T=100°C$, helium backing pressure $P=60$ psi, laser-to-nozzle distance $X\approx 30D$ (nozzle diameter $D\approx 70$ μm) and spectral resolution $R=8$ cm^{-1}.

3.2. Dispersed fluorescence spectra

3.2.1. Excitation of the 0_0^0 transition

The dispersed fluorescence spectra of the A- and C-isomer of *t*-stilbene/*n*-hexane (1:1) complexes recorded for 0_0^0 excitation are displayed in fig. 3. Both spectra have the same general features. The most prominent feature is a four-membered (A-isomer) and five-membered (C-isomer) progression of the low-frequency cluster mode X, already observed in the fluorescence excitation spectrum. The spacing of this progression is 17.2 ± 0.5 cm^{-1} for the A-isomer and 14.8 ± 0.5 cm^{-1} for the C-isomer. This progression is found to be repeated in intervals of 205 ± 1 cm^{-1} (A) and 204 ± 1 cm^{-1} (C). A look at the dispersed fluorescence spectrum of the 0_0^0 transition of the bare trans-stilbene molecule, given in fig. 3 for comparison, shows that this repetition of the low-frequency pattern is due to the combined excitation of overtones of the cluster mode X and overtones of the

symmetric in-plane ethylene bend mode ν_{25} of stilbene [39] in the ground electronic state of the cluster. The vast majority of bands detected in the dispersed fluorescence spectrum can be assigned to $25^0_m X^0_n$ transitions (see table 1).

The frequency spacing between overtones of this stilbene mode (205 cm^{-1}), as well as the relative intensity of these bands in the bare molecule, are found to be almost the same as in the cluster, indicating that this symmetric in-plane mode is only weakly affected by complexation. A much stronger perturbation of all out-of-plane stilbene modes, however, can be expected in the complex. A comparison of the dispersed fluorescence spectra shows that this is indeed the case. Neither the ethylenic carbon (C_e)-phenyl-out-of-plane bending mode ν_{36}, nor the very anharmonic, very low-frequency C_e-phenyl-out-of-plane twisting mode ν_{37} [39–42], or combinations thereof, can be found in the fluorescence spectra of the complexes. These are prominent, features in the low-energy region of the spectrum of the bare molecule [3,40].

Several low intensity bands can be resolved in the low-energy region of the fluorescence spectra of the A-isomer (table 1, see also fig. 4). These bands can be tentatively assigned to a second cluster mode Y ($\bar{\nu}$=76 cm^{-1}), and to combinations of this mode with the cluster mode X and ν_{25} ($25^0_m X^0_n Y^0_1$), although a conclusive assignment cannot be given without a normal mode analysis of the cluster [43].

Table 1
Assignment of the 0^0_0 level dispersed fluorescence spectrum of the A- and C-isomer of trans-stilbene/*n*-hexane (1:1) complexes

A-isomer			C-isomer		
frequency [a] (cm^{-1})	relative intensity	assignment [b]	frequency (cm^{-1})	relative intensity	assignment
0	0.67	$A0^0_0$	0	0.34	$C0^0_0$
17	1.00	AX^0_1	15	0.86	CX^0_1
35	0.59	AX^0_2	30	1.00	CX^0_2
52	0.18	AX^0_3	45	0.67	CX^0_3
76	0.07	AY^0_1(?)	59	0.24	CX^0_4
92	0.06	$AY^0_1X^0_1$	204	0.24	$C25^0_1$
205	0.57	$A25^0_1$	219	0.66	$C25^0_1X^0_1$
221	0.95	$A25^0_1X^0_1$	234	0.94	$C25^0_1X^0_2$
239	0.66	$A25^0_1X^0_2$	248	0.79	$C25^0_1X^0_3$
256	0.19	$A25^0_1X^0_3$	262	0.36	$C25^0_1X^0_4$
279	0.07	$A25^0_1Y^0_1$	282	0.18	?
297	0.12	$A25^0_1Y^0_1X^0_1$	407	0.09	$C25^0_2$
314	0.05	$A25^0_1Y^0_1X^0_2$	421	0.29	$C25^0_2X^0_1$
409	0.27	$A25^0_2$	436	0.47	$C25^0_2X^0_2$
426	0.55	$A25^0_2X^0_1$	453	0.53	$C25^0_2X^0_3$
443	0.42	$A25^0_2X^0_2$	467	0.25	$C25^0_2X^0_4$
460	0.14	$A25^0_2X^0_3$	625	0.06	$C25^0_3X^0_1$
485	0.02	$A25^0_2Y^0_1$	639	0.18	$C25^0_3X^0_2$
503	0.08	$A25^0_2Y^0_1X^0_1$	654	0.22	$C25^0_3X^0_3$
519	0.05	$A25^0_2Y^0_2X^0_1$	668	0.15	$C25^0_3X^0_4$
616	0.09	$A25^0_3$			
632	0.22	$A25^0_3X^0_1$			
649	0.19	$A25^0_3X^0_2$			
665	0.10	$A25^0_3X^0_3$			

[a] Frequencies are reported relative to the 0^0_0 transition of each isomer: $\bar{\nu}(A0^0_0)$=31855 cm^{-1}, $\bar{\nu}(C0^0_0)$=31970 cm^{-1} (see fig. 1, from ref. [28]).

[b] We use the following notation: $IY^l_k Z^n_m$, where I denotes the isomer (A or C), and Y and Z the vibrational modes. The sub- and superscripts indicate the number of vibrational quanta in the ground and excited state, respectively.

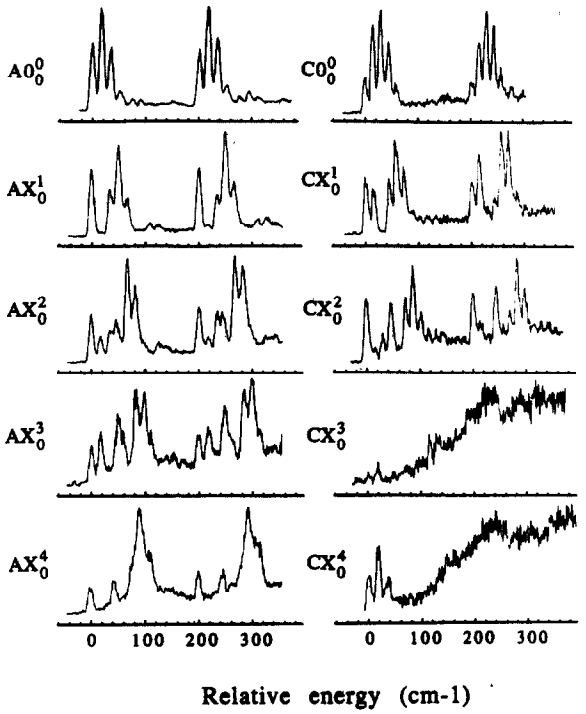

Fig. 4. Low-energy region (0 to 400 cm^{-1}) of the dispersed fluorescence spectra following excitation of the electronic origin 0_0^0 and overtones X_0^n, $1 \leqslant n \leqslant 4$, of the low-frequency cluster mode X in the A- and C-isomer of *t*-stilbene/*n*-hexane (1:1) complexes. All spectra have been recorded under the same experimental conditions: $T = 100$°C, $P(He) = 60$ psi, $X \approx 30D$, and $R = 8$ cm^{-1}.

3.2.2. Excitation of higher vibrational levels

Dispersed fluorescence spectra for nineteen vibrational levels in the S_1-state of the A- and C-isomer of trans-stilbene/*n*-hexane (1:1) complexes have been recorded. Excitation energy, wavelength, and assignment of the excited bands are given in table 2. For all of these levels, the excitation wavelength was red-shifted with respect to the origin of the bare stilbene molecule, so that the reported cluster spectra are mostly free from overlap with the fluorescence of the bare molecule. All spectra have been recorded with a spectral resolution of 8 cm^{-1} fwhm.

(a) *The A-isomer.* The fluorescence spectra recorded for excitation of overtones X_0^k ($0 \leqslant k \leqslant 4$) of the low-frequency cluster mode X are shown in fig. 4. In all cases a clear structured spectrum is observed, showing no sign of severe spectral congestion. One prominent feature of these spectra is a long low-frequency progression, which is repeatedly shifted by 200 cm^{-1}. All bands of the progression are assigned to transitions of the family $A25_m^0X_n^k$ ($0 \leqslant k \leqslant 4$, $0 \leqslant m \leqslant 1$, $0 \leqslant n \leqslant 9$). It will be shown below that the observed complex intensity pattern can be understood by performing a Franck–Condon analysis based on a shifted anharmonic oscillator model.

Table 2
Fluorescence decay times τ_f of trans-stilbene/*n*-hexane (1:1) complexes for total fluorescence detection. All measurements have been performed with monochromator slits fully open (fwhm = 5 nm) at a central detection wavelength of 332 nm

Transition	Energy [a] (cm^{-1})	τ_f (ns)
$A0_0^0$	0	2.79
AX_0^1	20	2.79
AX_0^2	40	2.79
AX_0^3	60	2.80
AX_0^4	80	2.78
AX_0^5	100	2.78
$C0_0^0$	115	2.80
CX_0^1	132	2.78
CX_0^2	149	2.78
CX_0^3	166	2.76
CX_0^4	183	2.78
$A25_0^1$	200	2.78
$A25_0^1X_0^1$	220	2.77
$A25_0^1X_0^2$	240	2.77
$A25_0^1X_0^3$	260	2.77
$A25_0^1X_0^4$	280	2.76
$A25_0^1X_0^5$	300	2.76
$C25_0^1$	315	2.76
$C25_0^1X_0^1$	332	2.76
$C25_0^1X_0^2$	349	2.75

[a] Energy relative to $\bar{\nu}(A0_0^0) = 31855$ cm^{-1}.

Several low-intensity bands are found between 100 and 200 cm^{-1} and above 300 cm^{-1}. As noted previously for the fluorescence spectrum of the 0_0^0 transition, these bands are tentatively assigned as $25_m^0X_n^kY_1^0$, where Y denotes a second, low-frequency cluster mode with $\bar{\nu} = 76$ cm^{-1}. We found no indication of the presence of a band attributable to a transition of the uncomplexed *t*-stilbene molecule in any of the spectra, so that dissociation of the complex can be ruled out at these energies. An assignment cannot be given for two bands found in the AX_0^2 (at 46 and 250 cm^{-1}) and AX_0^3 spectrum (at 59 and 263 cm^{-1}). The dispersed fluorescence spectrum for an excitation energy of 200 cm^{-1} ($A25_0^1$) shows again a struc-

tured spectrum, with the progression at low energies assigned to transitions $A25_0^1X_n^0$. Transitions $A25_1^1X_n^0$ are not detected, since the relative intensity of the transition 25_1^1 for the bare stilbene molecule is very low, as found in the fluorescence spectrum for this transition (not shown). However, $A25_2^1X_n^0$ transitions, shifted by 408 cm^{-1} relative to the $A25_0^1X_n^0$ progression, are observed, in agreement with the Franck–Condon analysis for this mode [3]. Some congestion of the spectrum is found in the energy range between 100 and 400 cm^{-1}, indicating a possible onset of fast IVR or severe mixing of the optically active modes.

A strikingly different fluorescence spectrum is monitored for excitation of the first combination band, $A25^1X_0^1$. Although the amount of excess energy is raised by only 20 cm^{-1} compared to $A25_0^1$, the spectrum shows almost complete congestion at this transition. Only the $A25_0^1X_n^1$ progression remains, albeit strongly reduced in intensity compared to the broadband relaxed fluorescence. This spectrum indicates that IVR is presumably faster than the fluorescence rate even at this very low excess energy of 220 cm^{-1} in the S_1 state of the cluster. We shall examine this point below with time-resolved studies.

The fluorescence spectra for excitation of the next overtone of the low-frequency cluster mode, $25_0^1X_0^2$, is even more congested; only two very weak isolated bands can be observed at this energy. The excitation of all higher overtones $25_0^1X_0^n$, $3 \leqslant n \leqslant 5$, leads to completely congested spectra without isolated bands. This onset of congested spectra for the excitation of combination bands $25_0^1X_0^n$ at excitation energies between 220 and 300 cm^{-1} above the origin of the A-isomer has to be compared with that of the bare stilbene molecule. For the latter, completely congested spectra are not observed at energies below the threshold for photoisomerization (≈ 1250 cm^{-1} [3,44,45]). In all spectra recorded at lower energies, well-resolved lines are present. The amount of spectral congestion in these spectra is generally found to increase with excess energy [3,4].

(b) *The C-isomer.* The dispersed fluorescence spectra of the C-isomer at low energies (excitation of CX_0^n, $0 \leqslant n \leqslant 2$) are very similar to those for the A-isomer at corresponding excess energies. Again structured spectra are recorded, showing no sign of spectral congestion. Prominent features are two low-frequency progressions CX_m^k and $C25_1^0X_m^k$. More members of these progressions are detectable than for the A-isomer, indicating a slightly larger displacement between the potential energy surfaces of the ground and the excited state in the C-isomer (see below).

Excitation of a higher overtone of the cluster mode, CX_0^3, does not lead to a sharp spectrum, but to an almost completely congested one. Some sharp features are still observable, but their intensity is very weak. The absorption band of the next higher overtone, CX_0^4, overlaps with a hot band of the A-isomer ($A25_0^1X_1^0$) and therefore the fluorescence spectrum for the transition CX_0^4 shown in fig. 4 is a combination of the spectrum of $A25_0^1$ and CX_0^4. The three distinct bands around 0 cm^{-1} in this spectrum are assigned as transitions $A25_0^1X_n^0$, $0 \leqslant n \leqslant 2$, and are found at the same wavelength as in spectrum $A25_0^1$ (fig. 5).

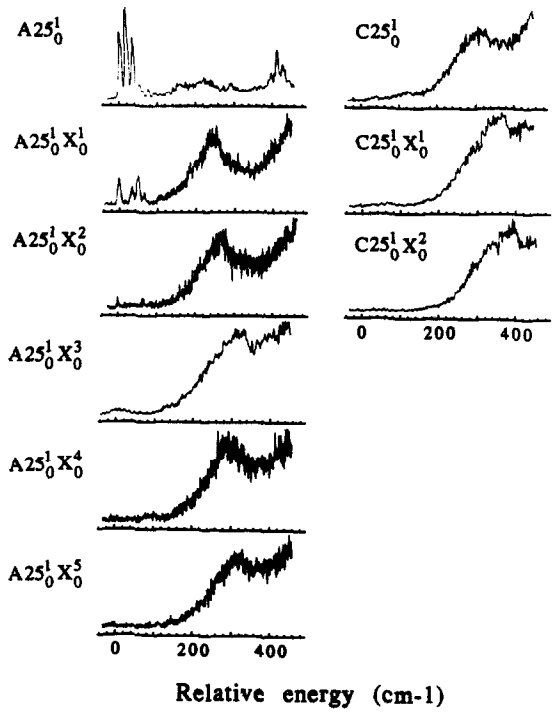

Fig. 5. Dispersed fluorescence spectra (0 to 500 cm^{-1}) following excitation of the symmetric in-plane ethylene bend mode ν_{25} and the combination bands $25_0^1X_0^n$, $1 \leqslant n \leqslant 5$, for the A- and C-isomer of *t*-stilbene/*n*-hexane (1:1) complexes. Experimental conditions as in fig. 4.

The rest of the spectrum can be assigned to the emission from CX_0^4 and is found to be slightly more congested than that for CX_0^3.

At higher excitation energies all measured spectra are congested without any unrelaxed (sharp) fluorescence structure. Attention is drawn to the fact that excitation of the in-plane stilbene mode ν_{25} yields a congested spectrum, indicating presumably rapid IVR for the C-isomer (see below), whereas for the A-isomer the corresponding spectrum is only slightly congested, and a clear structured spectrum is observed for the bare stilbene molecule.

3.3. Franck–Condon analysis and the potential

The prominent feature in the dispersed fluorescence spectra of the A- and C-isomer at low excitation energies is a long low-frequency progression assigned as X_m^k. In the following, the relatively complex intensity pattern of this progression will be examined by means of a Franck–Condon analysis. We follow the approach of Coon et al. [46] and Ansbacher [47]. It is assumed that the s normal coordinates of a polyatomic molecule in the electronically excited state q_i', $i=1, ..., s$, are given by a linear displacement d_i of the corresponding ground-state normal coordinate q_i'': $q_i'=q_i''+d_i$. The Franck–Condon overlap integral then separates into a product of one-dimensional overlap integrals, which, under the further assumption of harmonic oscillator wavefunctions in ground and excited states, are given by [46]

$$R(m,n)=(m!n!)^{1/2}2^{-(m+n-1)/2}\left(\frac{\beta}{1+\beta^2}\right)^{1/2}\times\left(\frac{1-\beta^2}{1+\beta^2}\right)^{(m+n)/2}\exp\left(-\frac{1}{2}\frac{\gamma^2\beta^2}{1+\beta^2}\right)\times\sum_{l=0}^{\min[m,n]}\left[\left(\frac{4\beta}{1-\beta^2}\right)^{l}\frac{(-\mathrm{i})^{m-l}}{l!(m-l)!(n-l)!}\times H_{m-l}(\mathrm{i}\beta^2\gamma(1-\beta^4)^{-1/2})\times H_{n-l}(-\beta\gamma(1-\beta^4)^{-1/2})\right]. \quad (1)$$

Here, m and n denote the vibrational quantum number in the excited and ground state, respectively. Furthermore H_{m-l} and H_{n-l} are Hermite polynomials, and

$$\alpha^2=\frac{4\pi^2c\bar{\nu}}{h},\quad \beta=\frac{\alpha''}{\alpha'},\quad \gamma=-\alpha' d, \quad (2)$$

where $\bar{\nu}$ is the vibrational frequency in cm^{-1}. The parameter d corresponds to the displacement between the minima in the electronic ground and excited state of the cuts through the potential energy surfaces along the mass-weighted normal coordinate q and is defined such that αd and, therefore, γ are dimensionless. A distortion factor $\gamma=2\sqrt{2\ln 2}$ then corresponds to a displacement d which is equal to the width (fwhm) of the wavefunction in the vibrationless excited state $\Delta q'$: $d=-\gamma\,\Delta q'/2\sqrt{2\ln 2}$.

The relative spectral intensities are then proportional to the square of the overlap integrals $|R(m,n)|^2$. The relative intensities for the bands of the low-frequency progression AX_n^m and CX_n^m, calculated on the basis of this model are in qualitative, but not quantitative, agreement with the measured dispersed fluorescence. For further improvement, we used anharmonic potentials for the ground and excited state with

$$V(x)=\tfrac{1}{2}m\omega^2x^2+\sigma\hbar\omega x^3. \quad (3)$$

Using first order perturbation theory, the anharmonic oscillator wavefunction in the eigenstate k is given as a sum of harmonic oscillator wavefunctions [48]:

$$|\psi_k\rangle=\sum_{i=-3}^{3}c_i|\varphi_{k+i}\rangle,$$

with

$$c_0=1,\quad c_1=-3\sigma\left(\frac{k+1}{2}\right)^{3/2},\quad c_2=0,$$

$$c_3=-\frac{\sigma}{3}\left(\frac{(k+3)(k+2)(k+1)}{8}\right)^{1/2},$$

$$c_{-1}=3\sigma\left(\frac{k}{2}\right)^{3/2},\quad c_{-2}=0,$$

$$c_{-3}=\frac{\sigma}{3}\left(\frac{k(k-1)(k-2)}{8}\right)^{1/2}. \quad (4)$$

To second order in the perturbation expansion, the energy of the eigenstate k is obtained:

$$E_k=(k+\tfrac{1}{2})\hbar\omega-\tfrac{15}{4}\sigma^2(k+\tfrac{1}{2})^2\hbar\omega-\tfrac{7}{16}\sigma^2\hbar\omega, \quad (5)$$

The relative spectral intensity is proportional to $|R_{anh}(m, n)|^2$, with $R_{anh}(m, n)$ given by

$$R_{anh}(m, n) = \sum_{i=-3}^{3} \sum_{j=-3}^{3} c_i^e c_j^g R(m+i, n+j) , \qquad (6)$$

where c_i^e and c_j^g are the coefficients in the expansion for the wavefunction of the excited and ground state (eq. (4)), and $R(m+i, n+j)$ is given by eq. (1), with $R(m, n) = 0$ for $m \leqslant 0$ or $n \leqslant 0$.

Figs. 6 and 7 show the low-frequency part of the measured spectra together with the model calculations for the A- and C-isomer, respectively. The displayed simulations have been performed with the following parameters, which gave the best agreement between experiment and calculation:

A-isomer:

$\bar{\nu}_g = 17.2 \pm 0.5\ \mathrm{cm}^{-1}$, $\bar{\nu}_e = 20.0 \pm 0.5\ \mathrm{cm}^{-1}$,

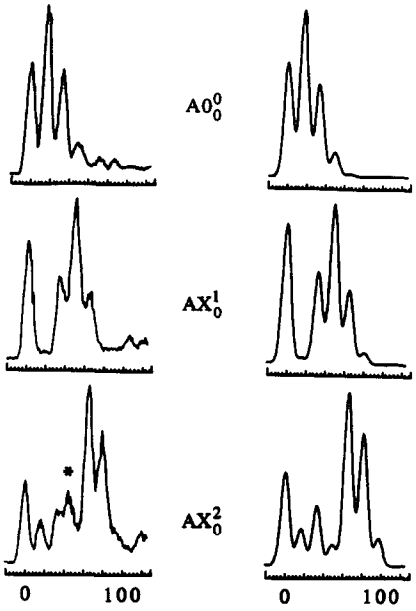

Fig. 6. Comparison of the dispersed fluorescence spectra AX$_0^n$, n=0, 1, 2 (left), with simulations (right) based on a Franck–Condon analysis (see text for details). The following parameters were used in the simulation: $\bar{\nu}_g = 17.2 \pm 0.5\ \mathrm{cm}^{-1}$, $\bar{\nu}_e = 20.0 \pm 0.5\ \mathrm{cm}^{-1}$, $\sigma_g = 0.028 \pm 0.005$, $\sigma_e = 0.025 \pm 0.005$, $\gamma = 1.60 \pm 0.05$. The highlighted band (*) in the spectrum AX$_0^2$ cannot be assigned to a transition AX$_m^n$.

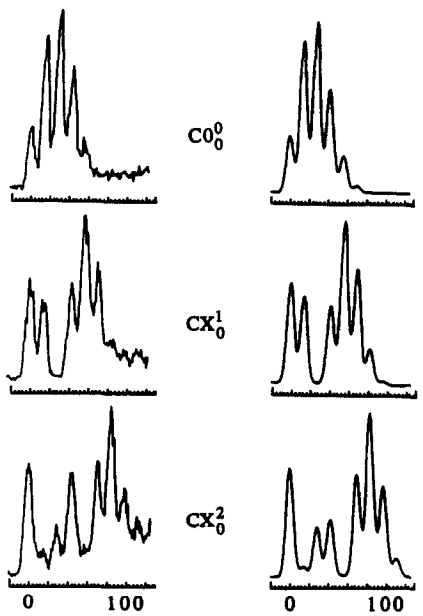

Fig. 7. Comparison of the dispersed fluorescence spectra CX$_0^n$, n=0, 1, 2 (left), with simulations (right) based on a Franck–Condon analysis (see text). The following parameters were used in the simulation: $\bar{\nu}_g = 14.7 \pm 0.5\ \mathrm{cm}^{-1}$, $\bar{\nu}_e = 17.8 \pm 0.5\ \mathrm{cm}^{-1}$, $\sigma_g = 0.025 \pm 0.008$, $\sigma_e = 0.020 \pm 0.005$, $\gamma = 2.25 \pm 0.05$.

$\sigma_g = 0.028 \pm 0.005$, $\sigma_e = 0.025 \pm 0.005$,

$\gamma = 1.60 \pm 0.05$.

C-isomer:

$\bar{\nu}_g = 14.7 \pm 0.5\ \mathrm{cm}^{-1}$, $\bar{\nu}_e = 17.8 \pm 0.5\ \mathrm{cm}^{-1}$,

$\sigma_g = 0.025 \pm 0.008$, $\sigma_e = 0.020 \pm 0.005$,

$\gamma = 2.25 \pm 0.05$.

The errors quoted above give a conservative estimation of the range over which each parameter has to be varied to give a significantly worse fit of the experimental data.

In general the calculated band intensities are in good agreement with the experimentally observed ones. For some bands, minor deviations between theory and experiment exist (see for example the intensity ratio of AX_3^1/AX_0^1 or the intensity CX_3^2) and these deviations becomes larger for higher vibrational quantum numbers in ground and excited states,

where the simple anharmonic model potential becomes a less accurate approximation of the real potential. It is also noted that the relative band intensities in the A- and C-isomer for the progression AX_m^k are slightly different from those for the progression $25_0^1A_m^k$, which is probably due to an anharmonic coupling between the 25 and X modes.

The Franck–Condon analysis presented above allows us to determine the parameters of an accurate anharmonic oscillator model potential for the low-frequency cluster mode X in both the ground and excited state. In the (presumably less strongly bound) C-isomer, the X normal coordinate shows a significantly larger displacement between ground and excited state than in the A-isomer, implying that the cluster excitation to its S_1 state induces a larger structural change in the C- than in the A-isomer.

4. Dynamics

4.1. Fluorescence rates: total fluorescence detection

The fluorescence lifetime for the vibrationless S_1 state of bare stilbene has been measured [3,16,44, 49,50] to be $\tau_f = 2.65 \pm 0.02$ ns. Fluorescence lifetimes for all absorption bands in the excitation spectrum of the A- and C-isomer are reported in table 3.

Table 3
Fluorescence decay times τ_f of trans-stilbene/*n*-hexane (1:1) complexes for single vibrational level detection in the regime of absent IVR

Transition	Energy [a] (cm^{-1})	Detection band [b] (cm^{-1})	Resolution (cm^{-1})	τ_f (ns)
$A0_0^0$	0	17	33	2.77
$A0_0^0$	0	222	33	2.78
AX_0^1	20	51	33	2.73
AX_0^2	40	68	33	2.71
AX_0^3	60	0	33	2.72
AX_0^4	80	48	33	2.65
AX_0^4	80	97	33	2.67
$C0_0^0$	115	231	25	2.76
$C0_0^0$	115	1850	33	2.79
CX_0^1	132	49	25	2.67
CX_0^2	149	90	33	2.73

[a] Energy relative to $\bar{\nu}(A0_0^0) = 31855\ cm^{-1}$.
[b] Detection wavelength given in cm^{-1} to the red of the excitation laser.

The detection of "total" fluorescence has been achieved by opening the monochromator slits completely and setting the detection wavelength far to the red of the excitation wavelength. The measured lifetimes of the hexane cluster are in excellent agreement with those recently reported by the Troe group [28]. As shown in fig. 8, a slight decrease in the fluorescence lifetimes can be observed as the vibrational energy in the S_1 state of the cluster is increased. Assuming that the fluorescence quantum yield in the cluster is equal to unity (as it is for the isolated molecule [51,52]), the fluorescence lifetimes of the vibrationless excited state are equal to the inverse of the radiative rate, which are then:

$$k_{rad}(\text{A-isomer}) = (0.358 \pm 0.003) \times 10^9\ s^{-1},$$

$$k_{rad}(\text{C-isomer}) = (0.357 \pm 0.003) \times 10^9\ s^{-1}.$$

Thus, the radiative rate of the $S_1 \rightarrow S_0$ transition in the cluster is slightly larger than that of the isolated molecule, $k_{rad}(\text{bare } t\text{-stilbene}) = 0.377 \times 10^9\ s^{-1}$. As has been pointed out by Strickler and Berg [53], and by Birks and Dyson [54,55], the radiative rate of the $S_1 \rightarrow S_0$ transition is approximately given by

$$k_{rad} = \frac{8\pi \times 2303}{c^2 N_A} \frac{n_f^3}{n_a} \langle \nu_f^{-3} \rangle_{av}^{-1} \int \frac{\epsilon}{\nu} d\nu, \qquad (7)$$

where n_f and n_a are the mean refractive indices of the solvent over the fluorescence and absorption spec-

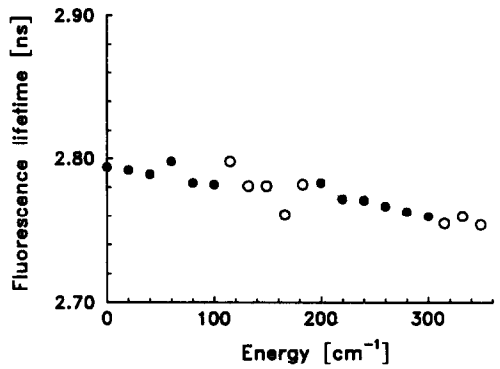

Fig. 8. Energy dependence of the fluorescence lifetime τ_f of the electronically excited configuration S_1 of *t*-stilbene/*n*-hexane complexes. Filled circles denote A-isomer, open circles C-isomer transitions. Total fluorescence detection has been achieved by opening the monochromator slits and setting the detection wavelength far to the red of the excitation wavelength (see text).

trum, respectively. In eq. (7), ν denotes the frequency of the optical transition in s^{-1}, and $\langle \nu_f^{-3} \rangle_{av}$ is the mean value of ν^{-3} over the fluorescence spectrum. Furthermore, ϵ is the molar extinction coefficient in $\ell\ mol^{-1}\ cm^{-1}$.

For isolated molecules and small clusters $n_f = 1$ and $n_a = 1$, thus the $\approx 5\%$ decrease in k_{rad} of the A-isomer can be attributed in part to a solvation effect on $\langle \nu_f^{-3} \rangle_{av}^{-1}$ and to the effect of the electrostatic interaction between the solute and the solvent molecule on the fluorescence spectrum. Knowing the red-shift of 380 cm^{-1} for the cluster, the first factor gives a decrease in k_{rad} in the cluster of 3.5%. The effect of the solvent on the fluorescence spectrum in small clusters can, in principle, be calculated by an extension of the model suggested by Shalev and Jortner for solute/rare-gas heteroclusters [56].

It should be mentioned that the effect of the refractive index on the radiative lifetime becomes important in clusters with dimensions much larger than the wavelength of the absorbed light and in solution.

The radiative lifetime of trans-stilbene in (3:2) methylcyclohexane/iso-hexane solvent has been found by Sumitami et al. to be $6.0 \times 10^8\ s^{-1}$ [57], which agrees closely with the value of $5.9 \times 10^8\ s^{-1}$ in *n*-pentane at 30°C calculated by Saltiel et al. using eq. (7) [58]. The refractive index of the solvent ($n = 1.36$ at 30°C and 403 nm [59]) thus induces an increase in the radiative rate by approximately a factor of $n^2 = 1.85$ and counteracts the decrease in the radiative rate due to the solvent effect on the fluorescence spectrum.

In the gas-phase measurements at 390 K of the Hochstrasser group [60,61], the lifetime of *t*-stilbene was found to be 15 ps at 265 nm and 55 ps at 287 nm excitation wavelength. In this case, the refractive index is one, but the laser excitation together with the thermal excitation induces a large excess energy in the molecule and the lifetime represents an average value over the energy distribution including isomerization at higher energies [62].

4.2. Time- and frequency-resolved fluorescence

4.2.1. Preliminaries: IVR in trans-stilbene

The dynamics of IVR in the bare trans-stilbene molecule have been characterized by Felker et al. [3–5] employing the same technique used in this study. The timescale of IVR in *t*-stilbene was shown to be strongly dependent on the amount of excess energy available, with a correlation to the increased density of states. At low energies ($< 600\ cm^{-1}$), with a density < 10, per cm^{-1}, IVR was found to be practically *absent* on the time scale of the fluorescence lifetime of the molecule. In an intermediate energy range ($600\ cm^{-1} < E < 1200\ cm^{-1}$), *restricted* IVR manifested itself by phase-shifted quantum beat modulated fluorescence decays. This regime corresponds to a case where the vibrational energy oscillates between the initially excited optically active level and a small number of energetically close "dark" states. At higher energies and at density-of-states of more than 150 per cm^{-1}, energy flow occurs practically irreversibly into a large number (typically $N > 10$) of vibrational levels, though some residual quantum beat modulation can still be observed. This *dissipative* regime is characterized by quasi-biexponential decays with a fast component on the order of tens of picoseconds.

The above sequence of three distinct IVR regimes, from *absent* to *restricted* to *dissipative* IVR, has been observed in a number of large molecules including anthracene [1–3], *n*-propyl-aniline [9], fluorene [7], azulene [8] and others, and seems to be established as a general characteristic of large polyatomic molecules.

4.2.2. IVR in t-stilbene/n-hexane (1:1) complexes

(a) *A-isomer.* In an attempt to characterize the IVR behavior of stilbene/hexane clusters, time- and frequency-resolved fluorescence detection has been performed for all 10 transitions observed in the fluorescence excitation spectrum of the A-isomer at excess energies ranging from 0 to 300 cm^{-1} (see figs. 9, 10, 13, 15, 17). Considering the good signal-to-background ratio in the fluorescence excitation spectrum, it is assumed that only single vibrational levels in the S_1-state have been excited.

For excitation of all overtones of the low-frequency cluster mode X (AX_0^n, $0 \leq n \leq 5$), single exponential decays have been observed (fig. 9), independent of the detection wavelength and resolution. This indicates that vibrational energy redistribution is essentially *absent* at these low excitation energies. A closer look at the experimental data (table 3) shows that for all excited overtones, the decay rates measured with single vibrational level (SVL) detection

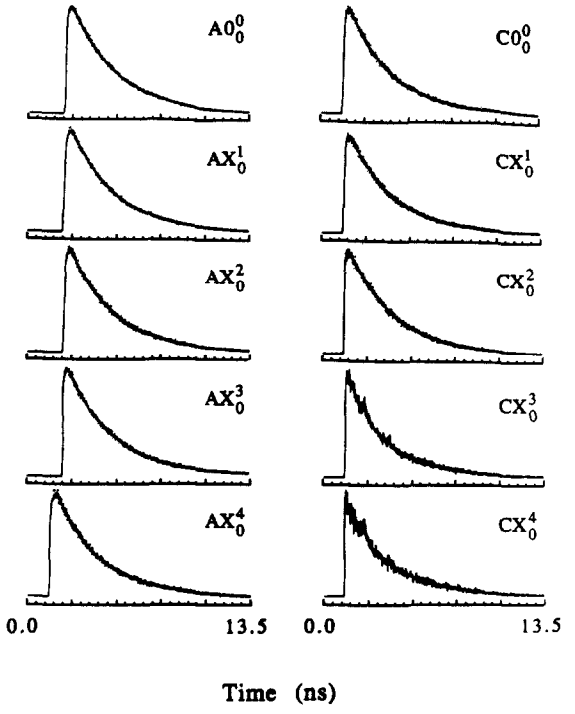

Fig. 9. Time- and frequency-resolved fluorescence decay profiles following excitation of the electronic origin 0_0^0 and overtones X_0^n, $1 \leqslant n \leqslant 4$, of the low-frequency cluster mode X in the A- and C-isomer of *t*-stilbene/*n*-hexane (1:1) complexes. For all measurements, the experimental conditions were the same as given in fig. 4. The detection wavelength (relative to the respective origin) and spectral resolution from top to bottom are: A-isomer: 17 and 33 cm^{-1}, 51 and 33 cm^{-1}, 68 and 33 cm^{-1}, 0 and 33 cm^{-1}, 48 and 33 cm^{-1}. C-isomer: 231 and 25 cm^{-1}, 49 and 25 cm^{-1}, 90 and 33 cm^{-1}, 20 and 33 cm^{-1}, 20 and 18 cm^{-1}. Fit parameters for these decays are given in tables 3 and 4.

are slightly faster than for total fluorescence detection. This indicates that energy redistribution between different cluster modes occurs on a timescale significantly longer than the radiative lifetime.

Excitation of the symmetric in-plane stilbene mode $A25_0^1$ leads to a biexponential decay for SVL detection with a fast lifetime $\tau_1 \approx 670$ ps and a second component $\tau_2 \approx 2.7$ ns (fig. 10). In contrast to the biexponential decays observed for the bare stilbene molecule at energies above 1200 cm^{-1}, the relative amplitude of the slow component is much larger than unity ($A_2/A_1 = 3.6$). This large amount of long-lived fluorescence is not due to detection of redistributed fluorescence since the dispersed fluorescence spectrum is clearly uncongested in this region and the detection resolution was sufficient to ensure single vibrational level detection.

Biexponential decays are characteristic for dissipative IVR; one optically active zero-order level $|s\rangle$ couples strongly with a manifold of N ($N \gg 1$) optically dark levels $\{|l\rangle\}$. If all these levels decay radiatively to the electronic ground state with a rate k_{rad}, the fluorescence decay for single vibrational level detection of the optically active state $|s\rangle$ is given as

$$I_s(t) \propto (N-1)\exp[-(k_{rad}+\Delta)t] + \exp(-k_{rad}t)\,, \tag{8}$$

where Δ corresponds to the rate of dissipative IVR. The above equation can be obtained quantum mechanically, and an analogous kinetic description is also possible [63] if we consider the coupling in the N levels as reversible and the system decaying by k_{rad}. In this case, Δ is simply the sum of forward and backward rate constants. Based on the above assumptions, the amplitude ratio of slow to fast component is $A_2/A_1 = 1/(N-1)$, thus being smaller than unity.

In the case of the biexponential transient observed for excitation of $A25_0^1$, however, $A_2/A_1 = 3.6$. Thus, the above IVR model (dissipative regime) does not account for the observed decay. In the $A25_0^1$ case, IVR can only occur by partitioning one high-energy, 200 cm^{-1} vibrational quantum of the stilbene mode ν_{25} into several quanta of low-frequency *intermolecular* vibrations. Once the energy has been transferred into the intermolecular modes, IVR is relatively more efficient within the manifold of intermolecular dark states $|c\rangle$. The low-frequency modes can exchange energy without large changes in the number of quanta involved. This is a sequential IVR process, where level coupling occurs between an optically active vibrational level $|a\rangle$ and an optically inactive state $|b\rangle$, which in turn couples to $|c\rangle$, etc. This state $|b\rangle$ differs in energy by $\Delta E = \hbar\omega$ (ω may be negative), and $|a\rangle$ and $|b\rangle$ are coupled via an interaction matrix element V_{ab}. Both levels can fluoresce to the ground state with a radiative rate k_{rad}. The strong coupling of $|b\rangle$ to a manifold of energetically accessible vibrational levels $\{|l\rangle\}$ is introduced phenomenologically by a nonradiative decay of $|b\rangle$ with a rate constant Γ (fig. 11). Such sequential IVR mechanisms were first observed in anthracene [1,2,5] and have found

Table 4
Prominent beat frequencies modulating the decays of trans-stilbene/*n*-hexane (1:1) complexes of figs. 9, 10 and 13

Transition	Energy [a] (cm^{-1})	Detection band [b] (cm^{-1})	Resolution (cm^{-1})	Frequencies $\omega/2\pi$ (GHz)
CX^3	166	20	33	0.77, 1.50
CX^4	183	20	18	0.76, 1.52
$A25^1X^1$	220	52	17	0.77, 1.71, 2.35
$A25^1X^1$	220	52	17	0.74, 1.75, 2.35
$A25^1X^2$	240	68	65	2.97, 1.29, 3.84
$A25^1X^3$	260	68	17	2.02

[a] Energy relative to $\bar{\nu}(A0_0^0) = 31855\ cm^{-1}$.
[b] Detection wavelength given in cm^{-1} to the red of the excitation laser.

Table 5
Decay parameters of the biexponential fluorescence decay profiles observed for trans-stilbene/*n*-hexane (1:1) complexes shown in figs. 10, 15 and 17

Transition	Energy (cm^{-1})	Detection band (cm^{-1})	Resolution (cm^{-1})	Decay parameters		
				τ_1 (ns)	τ_2 (ns)	A_2/A_1
$A25^1$	200	18	8	0.67	2.73	3.6
$A25^1$	200	18	11	0.56	2.80	2.9
$A25^1$	200	18	25	0.57	2.76	3.0
$A25^1X^4$	260	100	80	0.05	2.44	0.18
$A25^1X^5$	280	64	65	0.08	2.35	0.25
$C25^1$	315	87	80	0.07	2.40	0.15
$C25^1X^1$	332	76	80	0.06	2.03	0.12
$C25^1X^2$	349	76	80	0.04	2.45	0.23

[a] Energy relative to $\bar{\nu}(A0_0^0) = 31855\ cm^{-1}$.

a number of applications (see e.g. refs. [21,64]). The equations of time dependent perturbation theory in the interaction picture are then [48,65,66]:

$$i\hbar\dot{a} = V_{ab}e^{-i\omega t}b - \tfrac{1}{2}i\hbar k_{rad}a\,,$$
$$i\hbar\dot{b} = V_{ab}e^{i\omega t}a - \tfrac{1}{2}i\hbar(k_{rad}+\Gamma)b\,, \qquad (9)$$

where a and b denote the probability amplitude in states $|a\rangle$ and $|b\rangle$, respectively. The general solutions of eq. (9) are

$$a = A_1\exp(\mu_1 t) + A_2\exp(\mu_2 t)\,,$$
$$b = (i\hbar/V_{ab})\{(\mu_1+\tfrac{1}{2}k_{rad})A_1\exp[(\mu_1+i\omega)t] + (\mu_2+\tfrac{1}{2}k_{rad})A_2\exp[(\mu_2+i\omega)t]\}\,, \qquad (10)$$

with

$$\mu_{1,2} = -\frac{2k_{rad}+\Gamma+2i\omega}{4} \pm \frac{\sqrt{\Gamma^2-4\omega^2+4i\Gamma\omega-16V_{ab}^2}}{4}\,. \qquad (11)$$

The excitation of the optically active $|a\rangle$ state is represented by the initial conditions $a=1$, $b=0$, at $t=0$, and this gives

$$A_1 = \frac{\mu_2+\tfrac{1}{2}k_{rad}}{\mu_2-\mu_1}\,, \quad A_2 = -\frac{\mu_1+\tfrac{1}{2}k_{rad}}{\mu_2-\mu_1}\,. \qquad (12)$$

The fluorescence intensity for single-level detection of the optically active state $|a\rangle$ is proportional to

$$|a|^2 = |A_1\exp(\mu_1 t) + A_2\exp(\mu_2 t)|^2\,. \qquad (13)$$

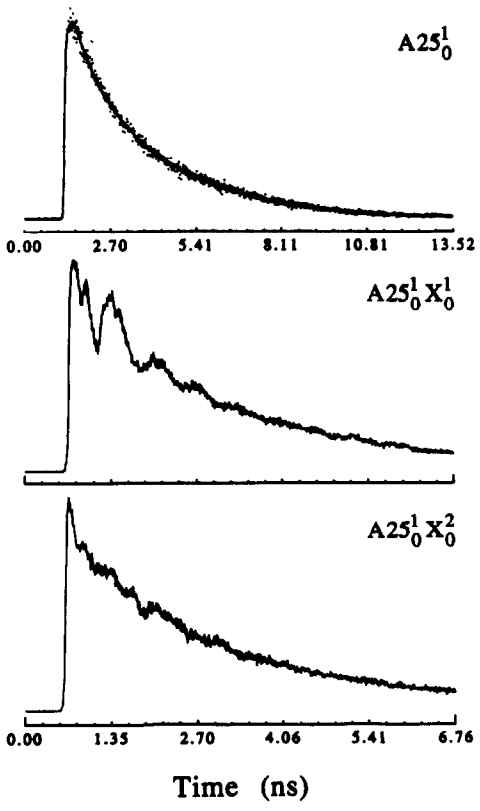

Fig. 10. Time- and frequency-resolved fluorescence decay of the A-isomer of *t*-stilbene/*n*-hexane complexes following excitation of (a) $A25_0^1$, together with biexponential fit ($\tau_1=0.67$ ns, $\tau_2=2.73$ ns, $A_2/A_1=3.6$). Detection wavelength (relative to the origin of the A-isomer) 18 cm^{-1}, spectral resolution 8 cm^{-1}. (b) $A25_0^1X_0^1$. Fourier analysis of the quantum-beat modulated decay reveals at least three modulation frequencies: $\nu_1=0.77$ GHz, $\nu_2=1.71$ GHz, $\nu_3=2.35$ GHz. Detection wavelength 52 cm^{-1}, spectral resolution 17 cm^{-1}. (c) $A25_0^1X_0^2$. Three beat frequencies are distinguished by Fourier analysis: $\nu_1=2.97$ GHz, $\nu_2=1.29$ GHz, $\nu_3=3.84$ GHz. Detection wavelength 68 cm^{-1}, resolution 65 cm^{-1}.

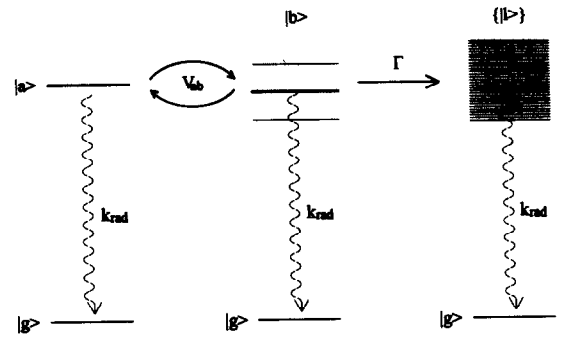

Fig. 11. Sequential model for IVR. The optically active level $|a\rangle$ is coupled via an interaction matrix element V_{ab} to an optically dark state $|b\rangle$. Both states can fluoresce to the electronic ground state $|g\rangle$ with a radiative rate k_{rad}. The strong coupling of $|b\rangle$ to a manifold of energetically nearby vibrational levels $\{|l\rangle\}$ is phenomenologically described by a nonradiative decay of $|b\rangle$ with a rate constant Γ.

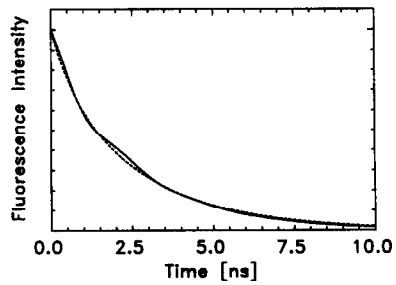

Fig. 12. Comparison of the observed biexponential decay for excitation of $A25_0^1$ (dotted line) to model calculations (solid line) using the sequential IVR model (see fig. 11 and text) with $k_{rad}=0.358\times10^9\,s^{-1}$, $V_{ab}=0.6$ GHz, $\omega=(E_b-E_a)/\hbar=2.5$ GHz, and $\Gamma=1.0\times10^9\,s^{-1}$. This corresponds to a coupling between the optically excited level $|a\rangle$ ($A25_0^1$) to the dark state $|b\rangle$ (intermolecular vibrational level), which is *weak* relative to the subsequent damping of $|b\rangle$ by vibronic coupling to the manifold of dark states $\{|l\rangle\}$.

Using this simplified picture, we can successfully model the observed decay for excitation of $A25_0^1$ if we choose the parameters $k_{rad}=0.358\times10^9$ s^{-1} (known), $V_{ab}=0.6$ GHz, $\omega=(E_b-E_a)/\hbar=2.5$ GHz, and $\Gamma=1.0\times10^9$ s^{-1} (fig. 12). To reproduce quasi-biexponential decays with the above model, the damping, introduced by the nonradiative decay rate Γ, has to be stronger than the effective vibrational coupling V_{ab} between states $|a\rangle$ and $|b\rangle$. This is consistent with the suggested physical picture in which the coupling between the intermolecular modes is facilitated compared to the coupling between the stilbene mode ν_{25} and the cluster modes, due to a large change in the number of vibrational quanta involved and/or the mismatch in energy. It should be noted that the above quantum mechanical treatment has a kinetic analogue, when we let a sequential process, with reversibility in the first step, proceed with the final rate being faster than the equilibration rate in the first step. Under this condition, the fast component would essentially be given by Γ and the slow one

by the equilibration rate, with the amplitude ratio of fast to slow now being less than one. It should be noted, however, that the quantum treatment is more appropriate, as these limits of extreme kinetic parameters are not exact and do not include the coherence in the system.

As shown in fig. 10, excitation of a combination of the stilbene mode ν_{25} with the low-frequency cluster mode, $A25_0^1X_0^1$, leads to a decay with strong quantum-beat modulation. Fourier analysis [2] of the signal reveals at least three beat frequencies (more beat frequencies might be obscured by noise), the most prominent of which has a frequency of 1.73 GHz, corresponding to a recurrence period of 580 ps. A somewhat less modulated decay is observed for excitation of the next overtone $A25_0^1X_0^2$ (fig. 10). Again, at least three beat frequencies can be identified by Fourier transformation, indicating that a number of modes are involved in the energy exchange.

The fluorescence decay underlying the modulation cannot be described by a single exponential with a lifetime equal to the inverse radiative rate. In both cases, for $A25_0^1X_0^1$ and $A25_0^1X_0^2$, the underlying decay is clearly multiexponential and fits well to a sum of two exponentials with lifetimes of 0.7 and 2.7 ns (relative amplitude of the fast component is 0.3), as found in the analysis of the decay of $A25_0^1$. This leads us to the conclusion that in the case of all three excited levels, the underlying biexponential decay is due to the energy flow out of the stilbene mode ν_{25} into the cluster vibrations and can be described in terms of the simple model (fig. 11) described above.

The quantum beat monitored for $A25X_0^3$ (fig. 13) is different in that only one frequency is prominent in the Fourier spectrum with $\nu = 2.02$ GHz, equivalent to a recurrence period of 495 ps. It is worth mentioning that more than ten recurrences have been monitored in this perfect example of quantum beats in clusters, indicating a coherent and reversible energy flow involving *t*-stilbene/*n*-hexane cluster modes.

To learn about the effect of the nature of the mode excited on the dynamics of $A25_0^1$ and $A25_0^1X_0^3$, we fitted the quantum beat for $A25_0^1X_0^3$ to eq. (13). A reasonable fit, especially of the first 3 ns, was obtained using the following parameter set: $k_{rad} = 0.358 \times 10^9$ s^{-1}, $V_{ab} = 4.9$ GHz, $\omega = (E_b - E_a)/\hbar = 8.0$ GHz, and

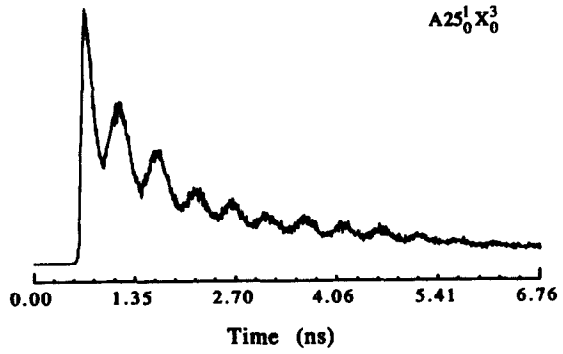

Fig. 13. Excitation of the combination band $A25_0^1X_0^3$ in the A-isomer showing quantum beats with a large modulation depth. The frequency of the modulation is 2.02 GHz, equivalent to a recurrence period of 495 ps. Fluorescence was detected at 68 cm^{-1} to the red of the excitation laser wavelength, the spectral resolution is 17 cm^{-1} and the other experimental conditions are similar to those of fig. 4.

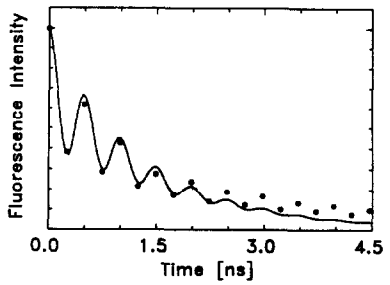

Fig. 14. Comparison of the observed quantum beats for excitation of $A25_0^1X_0^3$ (filled circles) to model calculations (solid line) using the sequential IVR model (see fig. 11 and text). The transitory behavior was obtained with $k_{rad} = 0.358 \times 10^9$ s^{-1}, $V_{ab} = 4.9$ GHz, $\omega = (E_b - E_a)/\hbar = 8.0$ GHz, and $\Gamma = 1.6 \times 10^9$ s^{-1}. This corresponds to a coupling between the optically excited level $|a\rangle$ ($A25_0^1X_0^3$) to the dark state $|b\rangle$, which is *strong* relative to the subsequent damping of $|b\rangle$ by vibronic coupling to the manifold of dark states $\{|l\rangle\}$.

$\Gamma = 1.6 \times 10^9$ s^{-1} (fig. 14). The main difference between this fit and the fit for $A25_0^1$ is the considerably larger coupling matrix element V_{ab}, corresponding to a largely accelerated IVR rate. We suggest that this acceleration occurs because four vibrational quanta are excited in $A25_0^1X_0^3$ and preferred pathways for energy redistribution are possible with no or relatively little change in the total number of vibrational quanta. The effective coupling is enhanced when cluster modes are matched on the solute.

By increasing the excitation energy further ($A25_0^1X_0^4$ and $A25_0^1X_0^5$), one monitors biexponential decays corresponding to dissipative energy redistribution (fig. 15). In both cases, the fast component of the decay was less than 100 ps (50 and 80 ps), indicating very rapid vibrational dynamics. From the amplitude ratio of fast to slow component (F/S) of 5.5 for $A25_0^1X_0^4$, it can be estimated that the number of coupled levels N is at least 6. This value can only serve as a lower limit, because the ratio F/S may appear too low through detection of vibrationally relaxed fluorescence, which is generally characterized by a single exponential decay constant equal to the radiative rate of the molecule (long component). In our case this seems highly probable in view of the complete congestion of the dispersed fluorescence spectrum and the relatively low detection resolution used in this experiment. The important point here is the development of the dissipative regime and, unlike lower quanta of X, the dominance of the fast component. The slight modulation which remains on the decay for $A25_0^1X_0^4$ is typical of excitation energies just high enough to observe dissipative behavior, as has been demonstrated in the case of isolated stilbene and anthracene molecules [1–5].

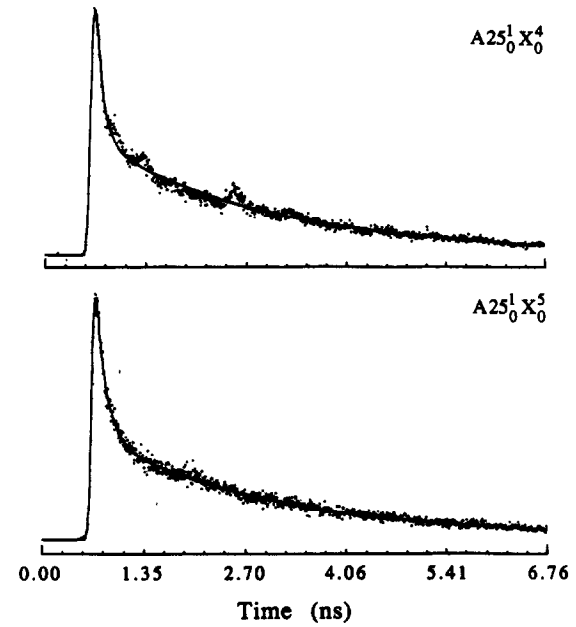

Fig. 15. Biexponential fluorescence decays observed for excitation of the A-isomer at excess energies of 280 and 300 cm^{-1}. (a) $A25_0^1X_0^4$. The decay is shown together with the best biexponential fit ($\tau_1=50$ ps, $\tau_2=2.44$ ns, $A_2/A_1=0.18$). The slight modulation observed is characteristic for excitation energies just high enough to observe dissipative IVR behavior. Detection wavelength relative to the origin of the A-isomer: 100 cm^{-1}, resolution: 80 cm^{-1}. (b) $A25_0^1X_0^5$: Parameters of the best biexponential fit are $\tau_1=80$ ps, $\tau_2=2.35$ ns, $A_2/A_1=0.25$. Detection wavelength: 64 cm^{-1}, resolution: 65 cm^{-1}. Experimental conditions as in fig. 4.

The cluster and the bare molecule have both similarities and striking differences in their IVR dynamics. Both exhibit the general regimes of IVR: *absent* IVR at low excess energies, manifested by single exponential decays, *restricted* IVR in an intermediate energy region with quantum-beat modulated decays, and *dissipative* IVR at high excess energies, identified by strongly biexponential decays. The excitation energies at which the three regimes are observed is, however, very different between the cluster and the isolated molecule. The bare stilbene molecule needs more than 600 cm^{-1} of vibrational energy to show quantum beats and more than 1200 cm^{-1} to reach the dissipative regime, whereas the corresponding energies are vastly decreased in the cluster. Quantum beats are found for energies between 220 and 260 cm^{-1}, and at higher energies IVR is dissipative. One important factor for this lies in the large number of low-frequency vibrations (large density-of-states) provided by the complexation. Currently a normal mode analysis of the intermolecular vibrations of stilbene/hexane complexes is not available so that a precise count of the density-of-states cannot be presented. To estimated the increase in the density-of-states on complexation, we calculated the density-of-states for stilbene/hexane complexes under the assumption that the frequencies of the intermolecular vibrations are the same as for a fairly similar complex, 2,5-diphenylfuran/*n*-hexane [36].

Estimates of the frequencies of the six van der Waals modes of this complex, based on atom–atom pair-potential calculations of the intermolecular potential, have been recently given by Mangle et al. as: 76, 9, 15, 18, 108, 78 cm^{-1} [36]. Using these frequencies, we find that the density-of-states exceeds 60 per cm^{-1} at an excess energy of 200 cm^{-1} (fig. 16). Considering the fact that in the isolated stilbene molecule restricted IVR is observed for a density-of-states between 10 per cm^{-1} and 150 per cm^{-1} and

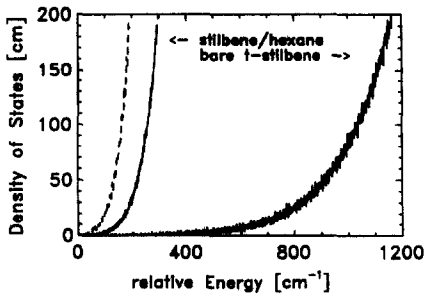

Fig. 16. Density-of-states for *t*-stilbene/*n*-hexane complexes and bare *t*-stilbene obtained by direct count [67]. For the vibrational modes of *t*-stilbene, we used the frequency set given by Negri et al. [68] and for the six intermolecular modes we used the frequencies given in the Appendix. The dashed line represents the density-of-states obtained by using the frequencies estimated by Mangle et al. [36] for 2,5-diphenylfuran/*n*-hexane (1:1) complexes results. Anharmonicity corrections were neglected. The energy is given relative to the origin of bare stilbene and stilbene/hexane, respectively.

IVR is dissipative for higher values, the increase in the density of states through complexation seems more than enough to account for the observed dissipative IVR above 260 cm^{-1}. This assumes that the mean coupling matrix elements between optically active and dark states in the cluster are at least comparable to those of the bare stilbene molecule. Even for intermolecular vibrational frequencies 50% higher than those used in the above estimation, the density-of-states would exceed 20 per cm^{-1} at 200 cm^{-1} and 100 per cm^{-1} at 300 cm^{-1}.

Out-of-phase quantum-beats have been observed in the case of bare *t*-stilbene and anthracene [1–5] through detection of relaxed fluorescence, but our attempts for the hexane cluster have not been successful. Contrary to the case of the bare *t*-stilbene and anthracene molecules, no sharp bands in the relaxed fluorescence of the cluster could be detected in the dispersed fluorescence spectra and this makes single vibrational level detection very difficult. For two excitation bands, $A25_0^1$ and $A25_0^1X_0^2$, a slight rise was found in the time-resolved decays when detecting the relaxed fluorescence, but the relative amplitude of the rising component was not large enough to allow an unambiguous determination of the corresponding time constant.

(b) *C-isomer.* A similar investigation of the IVR behavior in the C-isomer was performed by detecting the time- and frequency-resolved fluorescence for the transitions $CX_0^n (0 \leqslant n \leqslant 4)$, and $C25^1X_0^n (0 \leqslant n \leqslant 2)$. At low excitation energies (CX_0^n, $n \leqslant 2$) single exponential decays are observed, as in the case of the A-isomer (fig. 9). Interestingly, excitation of the next two overtones of this low-frequency cluster mode, CX_0^3 and CX_0^4, reveals beat-modulated decays, although the modulation is far less pronounced than in the case of the A-isomer. These quantum-beats represents a unique example of restricted energy redistribution between different cluster modes without an intramolecular mode being excited.

Excitation of the symmetric stilbene vibration $C25_0^1$ shows dissipative energy flow into the intermolecular vibrations on a time scale of less than 100 ps, which is faster than the rate found for the A-isomer. This dissipative energy relaxation becomes slightly more rapid for excitation of the combination bands $C25_0^1X_0^1$ and $C25_0^1X_0^2$ (fig. 17). We thus conclude that vibrational energy redistribution in the C-isomer again proceeds via the three distinguishable regimes, i.e. absent, restricted and dissipative. In comparison to the A-isomer, IVR is accelerated in the C-isomer. This is due, at least in part, to a lowering of the frequencies of intermolecular vibrations, as shown for the X-mode which has a frequency of 17 cm^{-1} in the C-isomer compared to 20 cm^{-1} in the excited state of A. Even a small decrease in the low-frequency intermolecular vibrational frequencies raises the density-of-states significantly, leading to faster IVR. The less rigid structure of the C-isomer, as revealed by a smaller red-shift and a larger displacement of the X normal coordinate between ground and excited state, should lead to larger amplitude motions, and hence larger anharmonicities for the coupling. However, more detailed analysis is needed to justify the magnitude of the couplings.

5. Conclusions

In this work, the picosecond dynamics of IVR in "solute/solvent" complexes of trans-stilbene and *n*-hexane was investigated using time- and frequency-resolved picosecond fluorescence spectroscopy. Due to the large binding energy and number of transitions in the fluorescence excitation spectrum, trans-stilbene/*n*-hexane (1:1) clusters provide a unique op-

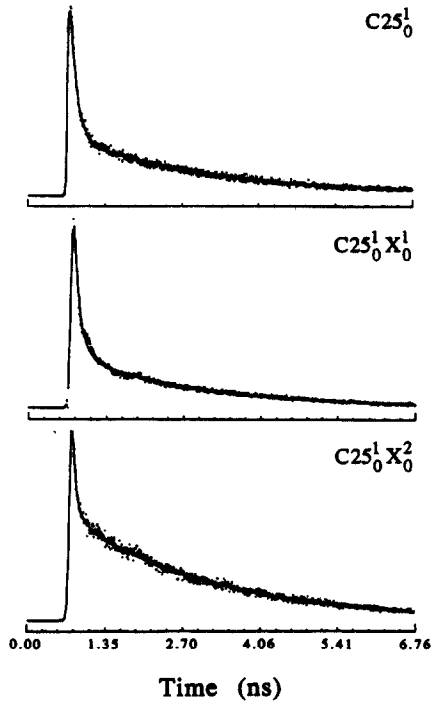

Fig. 17. The fluorescence decay profiles observed for excitation of $C25X_0^n$, $n=0, 1, 2$ at excess energies of 200, 217 and 234 cm^{-1} relative to the origin of the C-isomer. The data are shown together with the best biexponential fit with the following parameters: (a) $C25_0^1$: $\tau_1=70$ ps, $\tau_2=2.40$ ns, $A_2/A_1=0.15$. (b) $C25_0^1X_0^1$: $\tau_1=60$ ps, $\tau_2=2.03$ ns, $A_2/A_1=0.12$. (c) $C25_0^1X_0^2$: $\tau_1=40$ ps, $\tau_2=2.45$ ns, $A_2/A_1=0.23$. All experiments have been performed with a spectral resolution of 80 cm^{-1}. Fluorescence detection occurred at 87 cm^{-1} (a) and 76 cm^{-1} (b and c) to the red of the excitation laser wavelength.

portunity to follow the energy redistribution from the solute molecule to the intermolecular solute–solvent vibrations without vibrational predissociation.

As in the bare *t*-stilbene molecule, we identified and studied three different IVR regimes in this cluster. At low energies, no apparent vibrational redistribution of the optically excited level occurs on the timescale of the fluorescence lifetime. At intermediate energies, restricted IVR manifests itself through quantum-beat modulated fluorescence decays, whereas quasibiexponential decays at higher energy indicate the dissipative character of IVR. The mechanism of IVR involves sequential steps with an effective coupling depending on the solute or the cluster mode excited.

The striking difference between IVR behavior in the isolated molecule and in the complex is the extreme lowering of the amount of excess energy necessary for rapid energy redistribution. While the bare stilbene molecule must be excited to vibrational energies of at least 600 cm^{-1} to observe restricted IVR, quantum beats in the A-isomer of the complex were observed at energies between 200 and 240 cm^{-1} and between 60 and 80 cm^{-1} in the case of the C-isomer. At all higher energies, vibrational energy redistributes dissipatively on a timescale of tens of picoseconds. This factor of five decrease in the amount of energy needed for IVR to occur dissipatively compared to the bare stilbene molecule, where dissipative IVR sets in at 1200 cm^{-1}, is related to the increased density-of-states provided by the six low-frequency intermolecular cluster vibrations.

The coherent transfer of energy between the solute and cluster modes becomes evident in a quantum-beat pattern (up to ten recurrences) with a redistribution time of ≈ 500 ps. There is an interplay between the structure and the dynamics of IVR in the two isomers studied. Further studies of the dynamics are planned for the larger members of the cluster family.

Acknowledgement

One of us (ChL) gratefully acknowledges a postdoctoral fellowship from the Deutsche Forschungsgemeinschaft. This work was supported by a grant from the National Science Foundation.

Appendix

To deduce a structure for trans-stilbene/*n*-hexane, we have carried out atom–atom pair-potential energy calculations [#1] using intermolecular potentials of the Buckingham 6–exp–1 type:

$$V=\sum_i\sum_j\left(-\frac{A}{r_{ij}^6}+B\exp(-Cr_{ij})+\frac{q_iq_j}{r_{ij}}\right), \qquad (14)$$

and Lennard-Jones 6–12–1 type:

[#1] We are grateful to Professor Peter Felker and Dr. Paul Joireman for providing us with the energy minimization program.

$$V=\sum_i \sum_j \left(-\frac{A}{r_{ij}^6}+\frac{B}{r_{ij}^{12}}+\frac{q_i q_j}{r_{ij}}\right). \quad (15)$$

In these equations the Coulombic third term [69–71] provides a correction for the electrostatic interaction for non-uniform charge distributions. The potential parameters were taken from the work of Williams [69] and Scheraga [70]. The distribution of partial charges was also based on the work of Williams [69]. The partial charge of all H-atoms was assumed to be $q_H=-0.153$, whereas for the carbon atoms $q_C=-n_H q_H$, with n_H denoting the number of hydrogen atoms connected to the respective carbon atom.

The structural parameters of trans-stilbene in the electronic ground state were taken from the theoretical study of Negri et al. [68], and those of *n*-hexane from ref. [72]. We note that the excited state geometry is also planar [30,35], so that, as far as the calculations are concerned, the structures of trans-stilbene in the ground and excited electronic state are similar.

The most energetically favorable geometry of the cluster is characterized by the carbon atoms of the hexane molecule being located in a plane parallel to that spanned by the two phenyl rings, with its long axis parallel to the trans-stilbene long axis (see fig. 2). Using eq. (14) and the parameter set given in ref. [69], we find a binding energy for this configuration of 2040 cm^{-1}, whereas the use of eq. (15) with the parameters taken from ref. [70] results in a binding energy of 2260 cm^{-1}.

We note that for this specific cluster the introduction of the Coulombic term in eqs. (14) and (15) has no effect on the most energetically favorable configuration. Here, the Coulombic energy, which is on the order of 100 cm^{-1}, is much smaller than the attractive and repulsive energies calculated from the first and second term of eqs. (14) and (15).

This energetically favorable configuration is denoted as isomer A. The potential energy calculations predict the existence of a second stable isomer (labeled isomer C), with a binding energy of 2170 cm^{-1} (eq. (15)). This configuration differs in that the hexane molecule is rotated by 180° around its long axis, and that the long axes of the molecules are no longer parallel to each other. The distance between the center of mass of both molecules (3.72 Å using eq. (15)) is also slightly larger than for configuration A (3.67 Å).

The above binding energies should be regarded as estimates. Our purpose here is to illustrate the consistency of the larger spectral red shift for hexane complexes as compared to, e.g., rare gas complexes under normal conditions. The structures are consistent with recent rotational coherence experiments [28, see text] and more refinement can be done in further experimental studies.

As an extension of the above calculation we have also obtained the eigenfrequencies of the six cluster normal modes, following the external force field method outlined by Bernstein [43]. Using eq. (15) together with Scheraga's parameter set, these frequencies are: 17, 19, 23, 50, 77, and 154 cm^{-1}.

In a Cartesian coordinate system where the *x*-axis points along the stilbene long axis, the *y*-axis lies in the plane spanned by the stilbene molecule and *z*-axis connects the center-of-mass of stilbene and hexane in the equilibrium A-configuration, the two lowest eigenfrequencies correspond to vibrational motions along the *y*- and *x*-axis, respectively. The third eigenvalue, 22 cm^{-1}, represents a torsional motion around the *z*-axis, and the fifth, 77 cm^{-1}, a vibrational motion along the *z*-axis. The two remaining eigenfrequencies correspond to "out-of-plane" torsions, where the two molecules leave the preferred parallel configuration.

References

[1] W.R. Lambert, P.M. Felker and A.H. Zewail, J. Chem. Phys. 75 (1981) 5958; 81 (1984) 2217.

[2] P.M. Felker and A.H. Zewail, J. Chem. Phys. 82 (1985) 2961, 2975, 2994.

[3] J.A. Syage, W.R. Lambert, P.M. Felker, A.H. Zewail and R.M. Hochstrasser, Chem. Phys. Letters 88 (1982) 266; J.A. Syage, P.M. Felker and A.H. Zewail, J. Chem. Phys. 81 (1984) 4685, 4706.

[4] P.M. Felker, W.R. Lambert and A.H. Zewail, J. Chem. Phys. 82 (1985) 3003.

[5] P.M. Felker and A.H. Zewail, Advan. Chem. Phys. 70 (1988) 265.

[6] A.J. Kaziska, S.A. Wittmeyer, A.L. Motyka and M.R. Topp, Chem. Phys. Letters 154 (1989) 199.

[7] J.F. Kauffman, M.J. Côté, P.G. Smith and J.D. McDonald, J. Chem. Phys. 90 (1989) 2874.

[8] D.R. Demmer, J.W. Hager, G.W. Leach and S.C. Wallace, Chem. Phys. Letters 136 (1987) 329.
[9] J.S. Baskin, M. Dantus and A.H. Zewail, Chem. Phys. Letters 130 (1986) 473.
[10] G.A. Bickel, D.R. Demmer, G.W. Leach and S.C. Wallace, Chem. Phys. Letters 145 (1988) 423.
[11] C. Lakshminarayan and J.L. Knee, J. Phys. Chem. 94 (1990) 2637.
[12] P.G. Smith and J.D. McDonald, J. Chem. Phys. 92 (1990) 1004.
[13] P.G. Smith and J.D. McDonald, J. Chem. Phys. 96 (1992) 7344.
[14] A.J. Kaziska and M.R. Topp, Chem. Phys. Letters 180 (1991) 423.
[15] L.W. Peng, B.W. Keelan, D.H. Semmes and A.H. Zewail, J. Phys. Chem. 92 (1988) 5540.
[16] L. Bañares, A.A. Heikal and A.H. Zewail, J. Phys. Chem. 96 (1992) 4127.
[17] D.M. Willberg, M. Gutmann, E.E. Nikitin and A.H. Zewail, Chem. Phys. Letters 201 (1993) 506.
[18] M. Gutmann, D.M. Willberg and A.H. Zewail, J. Chem. Phys. 97 (1992) 8048.
[19] M. Gutmann, D.M. Willberg and A.H. Zewail, J. Chem. Phys. 97 (1992) 8037.
[20] D.M. Willberg, M. Gutmann, J.J. Breen and A.H. Zewail, J. Chem. Phys. 96 (1992) 198.
[21] D.H. Semmes, J.S. Baskin and A.H. Zewail, J. Chem. Phys. 92 (1990) 3359.
[22] A. Heikal, L. Bañares, D.H. Semmes and A.H. Zewail, Chem. Phys. 156 (1991) 231.
[23] M.R. Nimlos, M.A. Young, E.R. Bernstein and D.F. Kelley, J. Chem. Phys. 91 (1989) 5268.
[24] J.J.F. Ramaekers, H.K. van Dijk, J. Langelaar and R.P.H. Rettschnick, Faraday Discussions Chem. Soc. 75 (1983) 183;
M. Heppner and R.P.H. Rettschnick, in: Structure and dynamics of weakly bound complexes, ed. A. Weber (Reidel, Dordrecht, 1987) p. 553.
[25] P.M. Weber and S.A. Rice, J. Chem. Phys. 88 (1988) 6120.
[26] A.J. Kaziska, S.A. Wittmeyer and M.R. Topp, J. Phys. Chem. 95 (1991) 3663.
[27] M. Topp, Intern. Rev. Phys. Chem. 12 (1993) 149.
[28] Ch. Lienau, Ph.D. Dissertation, Göttingen (1992);
Ch. Lienau, J. Schroeder, J. Troe and K. Wack, to be published.
[29] J.S. Baskin, P.M. Felker and A.H. Zewail, J. Chem. Phys. 86 (1987) 2483.
[30] J.S. Baskin and A.H. Zewail, J. Phys. Chem. 93 (1989) 5701.
[31] D.V. O'Connor and D. Phillips, Time-correlated single photon counting (Academic Press, London, 1984).
[32] P.R. Bevington, Data reduction and error analysis for the physical sciences (McGraw-Hill, New York, 1969).
[33] D.W. Marquardt, J. Soc. Ind. Appl. Math. 11 (1963) 431.
[34] T. Zwier, M.E. Carrasquillo and D.H. Levy, J. Chem. Phys. 78 (1984) 5493.
[35] B.B. Champagne, J.F. Pfanstiel, D.F. Plusquellic, D.W. Pratt, W.M. van Herpen and W.L. Meerts, J. Phys. Chem. 94 (1990) 6.
[36] E.A. Mangle, A.L. Motyka, P. Salvi and M.R. Topp, Chem. Phys. 112 (1987) 443.
[37] D.H. Waldeck, Chem. Rev. 91 (1991) 415.
[38] A.J. Kaziska, M.I. Shchuka and M.R. Topp, Chem. Phys. Letters 183 (1991) 552.
[39] A. Warshel, J. Chem. Phys. 62 (1975) 214.
[40] L.H. Spangler, R. van Zee and T.S. Zwier, J. Phys. Chem. 91 (1987) 2782.
[41] T. Urano, H. Hamaguchi, M. Tasumi, K. Yamanouchi, S. Tsuchiya and T.L. Gustafson, J. Chem. Phys. 91 (1989) 3884.
[42] T. Suzuki, N. Mikami and M. Ito, J. Phys. Chem. 90 (1986) 6431.
[43] S. Li and E.R. Bernstein, J. Chem. Phys. 95 (1991) 1577.
[44] T.J. Majors, U. Even and J. Jortner, J. Chem. Phys. 81 (1984) 2330.
[45] J. Troe, Chem. Phys. Letters 114 (1985) 241.
[46] J.B. Coon, R.E. DeWames and C.M. Loyd, J. Mol. Spectry. 8 (1962) 285.
[47] F. Ansbacher, Z. Naturforsch. A 14 (1959) 889.
[48] C. Cohen-Tannoudji, B. Diu and F. Laloë, Quantum mechanics, Vols. I and II (Wiley, New York, 1977).
[49] Ch. Lienau, J. Schroeder, J. Troe and K. Wack, J. Chem. Phys., to be published.
[50] P.M. Felker and A.H. Zewail, J. Phys. Chem. 89 (1985) 5402.
[51] M. Sonnenschein, A. Amirav and J. Jortner, J. Phys. Chem. 88 (1984) 4214.
[52] A. Amirav and J. Jortner, Chem. Phys. Letters 95 (1983) 295.
[53] S.J. Strickler and R.A. Berg, J. Chem. Phys. 37 (1962) 814.
[54] J.B. Birks and D.J. Dyson, Proc. Roy. Soc. A 275 (1963) 135.
[55] J.B. Birks, in: Photophysics of aromatic molecules (Wiley–Interscience, New York, 1970).
[56] E. Shalev and J. Jortner, Chem. Phys. Letters 178 (1991) 31.
[57] M. Sumitani, N. Nakashima, K. Yoshihara and S. Nagakura, Chem. Phys. Letters 51 (1977) 183.
[58] A. Marinari and J. Saltiel, Mol. Photochem. 7 (1976) 225.
[59] Landolt–Börnstein, Zahlenwerte und Funktionen aus Naturwissenschaften und Technik, Neue Serie, Vol II, pt. 8 (Springer, Berlin, 1961).
[60] B.I. Greene, R.M. Hochstrasser and R.B. Weisman, Chem. Phys. 48 (1980) 289.
[61] R.M. Hochstrasser, Pure Appl. Chem. 52 (1980) 2683.
[62] J.W. Perry, N.F. Scherer and A.H. Zewail, Chem. Phys. Letters 103 (1983) 1.
[63] A. Frad, F. Lahmani, A. Tramer and C. Tric, J. Chem. Phys. 60 (1974) 4419.
[64] A.A. Stuchebrukhov and R.A. Marcus, in: Proceedings of the Berlin Conference on Femtosecond Chemistry, Berlin, 1993.
[65] W.E. Lamb Jr. and R.C. Retherford, Phys. Rev. 79 (1950) 549.
[66] T.E. Orlowski and A.H. Zewail, J. Chem. Phys. 70 (1979) 1390.

[67] T. Beyer and D.F. Swinehart, Commun. Assoc. Comput. Mach. 16 (1973) 379.
[68] F. Negri, G. Orlandi and F. Zerbetto, J. Phys. Chem. 93 (1989) 5124.
[69] D.E. Williams and T.L. Starr, Comput. Chem. 1 (1977) 173; D.E. Williams, Acta Cryst. A 31 (1975) 56; 36 (1980) 715.
[70] G. Nemethy, M.S. Pottle and H.A. Scheraga, J. Phys. Chem. 87 (1983) 1883;
F.A. Momany, L.M. Carruthers, R.F. McGuire and H.A. Scheraga, J. Phys. Chem. 78 (1974) 1595.
[71] K.S. Law and E.R. Bernstein, J. Chem. Phys. 82 (1985) 2856.
[72] Landolt–Börnstein, Zahlenwerte und Funktionen aus Naturwissenschaften und Technik, Neue Serie, Vol. II, pt. 7 (Springer, Berlin, 1976).